



An Adaptive Method to Estimate Evapotranspiration using Satellite and Reanalysis Products

Haneen Muhammad¹, Klara Finkele², Pádraig Flattery², Caren Jarmain³, Gary Lanigan⁴, and Conor Sweeney¹

Correspondence: Haneen Muhammad (haneen.muhammad@ucdconnect.ie)

Abstract. Accurate estimation of evapotranspiration (ET) is critical for hydrological, agricultural, and climate-related applications. However, spatially and temporally consistent ET datasets are often limited, particularly in regions like Ireland, where cloud cover is high and ground-based observations are sparse. This study evaluates ten global, operational open-access ET products by comparing them to Penman-Monteith (PM) reference values derived from weather station data across 22 locations in Ireland between 2019 and 2023. Systematic errors were identified in all ET products, varying across sites, seasons, and years. An adaptive bias correction (AB) method was applied, which dynamically adjusts each product based on recent errors. Although the AB method significantly improved individual ET estimates, no single product consistently exhibited superior performance under all conditions. To further enhance ET accuracy, a novel Combination (COM) method was introduced. This method assigns dynamic weights to each bias-corrected ET product based on recent skill scores, enabling the creation of an optimally merged ET estimate. Unlike traditional static statistical methods, which are interpretable but inflexible, and machine learning approaches, which are adaptive but opaque and data-intensive, the COM method offers a transparent, computationally efficient, and interpretable solution. It requires minimal historical data and runs efficiently on non-specialised systems, making it particularly suitable for operational settings. Results show that the merged COM product outperformed all individual ET datasets, achieving lower errors and stronger correlations with PM observations. Given the persistent cloud cover and variable satellite retrieval accuracy in regions like the Ireland, the ability to adapt to recent performance represents a significant advancement. Overall, the proposed adaptive merging framework provides a scalable, lightweight solution for improving ET monitoring. This method holds promise for enhancing operational hydrology, agricultural decision-making, and climate impact assessments in Ireland and other regions facing similar challenges.

1 Introduction

Evapotranspiration (ET) is a vital part of the hydrological cycle, governing the transfer of water from the land surface—such as open water, ice, soil, and vegetation—into the atmosphere and influencing local climate patterns (IPCC, 2023). It encompasses

¹School of Mathematics and Statistics, UCD Dublin, Ireland

²Met Éireann, Glasnevin Hill, Dublin, Ireland

³Centre for Geographical Analysis, Department of Geography and Environmental Studies, Stellenbosch University, South Africa

⁴Teagasc, Environmental Research Centre, Johnstown Castle, Wexford, Ireland



30



both evaporation from soil, plant canopies, and water bodies, and transpiration from plant leaves through stomata. Transpiration is linked to both total leaf area and plant water relations, with stomatal conductance responding to environmental factors, such as temperature, humidity, solar radiation and CO2 concentration (Collatz et al., 1991) and leaf area infuleced by land-use and land management activities (Khattak et al., 2025).

ET provides a crucial link between the surface energy balance (including micrometeorology and the atmospheric boundary layer) and the soil water balance (involving rainfall and hydrological components). ET influences near-surface temperature and boundary-layer development through latent and sensible heat partitioning as well as entrainment effects (Stap et al., 2014). It accounts for approximately 60% of terrestrial precipitation, making it the dominant component of the water balance in many vegetated landscapes (Katul et al., 2012). As climate change alters these environmental conditions, resulting shifts in transpiration and overall ET rates underscore the importance of reliable ET estimates for understanding the water balance, supporting sustainable water resource management, agriculture, and enhancing resilience to a changing climate (Wanniarachchi and Sarukkalige, 2022).

Eddy covariance systems (commonly referred to as flux towers) provide aerially averaged ground-based measurements of ET for a footprint area, but their complexity and high-cost limits extensive operational implementation. Several flux towers, monitoring CO2 and ET fluxes over a range of land uses, have been installed across Ireland in recent years (Richards et al., 2023). Unfortunately, a long-term, gap-filled dataset was not available for use in this study. Hence, we generated a multi-year field-level ET dataset for grass to benchmark the accuracy of remotely sensed ET at locations across Ireland. We used the Penman–Monteith (PM) equation (Allen et al., 1998) and Met Éireann weather station data as input for each point. The PM model integrates temperature, humidity, wind speed, and solar radiation, and is widely recognized for its strong theoretical foundation and has been extensively validated (Westerhoff, 2015; Amazirh et al., 2017). Endorsed by the Food and Agriculture Organization (FAO) as the standard method for calculating reference evapotranspiration (ET_o) due to its accuracy across diverse climates (Allen et al., 1998), the PM equation is also recommended for crop water requirements (Cai et al., 2007) and is commonly used in the literature for evaluation (Chen et al., 2005). The PM equation has also been applied with remote sensing data, combining energy balance and mass transfer approaches through resistance or conductance factors to improve ET accuracy across diverse climates and land covers (García-Gutiérrez et al., 2021). Its robust basis and broad use make it a reliable standard for assessing remotely sensed ET in the absence of ground observations.

Remote sensing and reanalysis products provide ET estimates with broad spatial coverage, making them particularly useful for regions with sparse ground-based measurements (Li et al., 2009). However, these products are subject to uncertainties, as their accuracy depends on factors such as sensor limitations, retrieval algorithms, and input data quality (Tran et al., 2023). Consequently, their reliability can vary across different locations, seasons, and weather conditions. In areas of persistent and extensive cloud cover which results in missing data, ET estimates are often interpolated or infilled (Li et al., 2021; Song et al., 2021).

To quantify the uncertainty of available ET products and produce more accurate estimates, several studies have employed data fusion techniques combining ET products from different sources (Wang et al., 2022a). These efforts have utilized diverse methodological approaches, with statistical methods being particularly well-studied.





One commonly used statistical method is Bayesian Model Averaging (BMA), which assigns probabilistic weights to different models based on their performance (Yao et al., 2014, 2016; Feng et al., 2016; Kazemi et al., 2021; Zhu et al., 2016; Wang et al., 2021a). Simple Taylor Skill fusion (STS) has also been applied, optimally combining datasets based on Taylor skill scores (Yao et al., 2017; Wang et al., 2021b; Baik et al., 2018, 2019). The Triple Collocation (TC) method has proven particularly valuable for estimating error variances among three independent datasets (Wang et al., 2024; Cui et al., 2023; Park et al., 2023; Li et al., 2022, 2023, 2024a, b; Cheng et al., 2024; He et al., 2020). Other statistical methods include the Empirical Orthogonal Function (EOF) approach (Feng et al., 2016), Modified Kling-Gupta Efficiency (KGE) fusion (Baik et al., 2019), Maximize R method (Baik et al., 2018), and Reliability Ensemble Averaging (REA) (Lu et al., 2021).

Statistical methods, while more interpretable, generate static datasets that cannot adapt to recent errors - a particular limitation in regions like Ireland where persistent cloud cover affects satellite-based ET accuracy. Recent years have seen growing application of machine learning approaches, including deep learning-based multimodal ensemble methods (Guo et al., 2024), artificial neural networks (ANNs) (Chen et al., 2020), and extremely randomized trees (ERT) (Shang et al., 2020). However, these methods often entail high computational costs and function as "black-box" models, limiting interpretability of errors and uncertainties.

To address these limitations, this paper presents a novel approach that avoids both machine learning and static techniques. The proposed method is computationally efficient, requires minimal historical data, runs on non-specialised systems, and dynamically adjusts to recent skill scores while maintaining transparency in optimally merging ET products. This approach is detailed through a description of the datasets used and the data preparation process, including standardization and aggregation. This is followed by performance comparisons using skill scores (Error, Bias, Root Mean Squared Error, and Correlation Coefficient) and adaptive bias preprocessing—comprising bias removal (seasonal correction) and adaptive combination (dynamic weighting). We then present the results before and after bias correction and combination, and provide methodological and product-level insights, highlighting the benefits and potential of the proposed approach.

2 Data

Data were extracted for the period 2019–2023, the earliest interval where all 10 ET products overlapped completely. Although 2018 also offered full coverage, it was excluded to avoid bias from that year's extreme European heatwave. Validation data were calculated for the selected period to ensure temporal consistency.

2.1 Satellite-based ET Products

2.1.1 LSA_SAF

5 The LSA-SAF DMET product (LSA) (Ghilain et al., 2011, 2012) provides daily ET estimates at a 3 km spatial resolution using ECMWF's H-TESSEL land surface model. It integrates SAF (Trigo et al., 2011) radiation, soil, and vegetation products





from the MSG satellite, ECMWF meteorological forecasts, and the ECOCLIMAP (Champeaux et al., 2006) land cover data. LSA-SAF DMET defines ET as the sum of evaporation from all surfaces (soil, plants, water bodies) and transpiration.

2.1.2 GLEAM

GLEAM Version 4.1a (GLEAM) (Miralles et al., 2025) provides daily ET estimates at a ~9 km spatial resolution. It integrates meteorological inputs from weather datasets downscaled from ERA5, vegetation inputs from different satellites including MODIS and Landsat, a soil moisture dataset that incorporates SAF soil moisture, and HiHydroSoil (Simons et al., 2020) land cover data. The GLEAM E (actual evaporation) variable is defined as the sum of transpiration, interception loss, evaporation from bare soil, open-water surfaces, snow sublimation and surface condensation.

95 2.1.3 MOD16

The two MOD16 products (MYD16A2GF from AQUA (AQUA) and MOD16A2GF from TERRA (TERRA)) (Mu et al., 2007) provide global ET estimates at a 500 m spatial resolution and an 8-day temporal resolution using an algorithm based on the Penman-Monteith equation. They integrate daily meteorological data from MERRA's GMAO reanalysis and satellite vegetation data from the MODIS and VIIRS sensors. The ET estimates from both the AQUA and TERRA products were used. They define ET as the sum of transpiration, interception losses and evaporation from soil.

2.1.4 WaPOR

WaPOR Version 3 (WaPOR)(FAO, 2020) provides dekadal (10 days) global ET estimates at a 300 m resolution using a Penman-Monteith based model. It incorporates meteorological inputs from GAMO's GEOS-5 and ERA5, along with land and vegetation data from VIIRS, Landsat, Sentinel, and MSG sensors and WorldCover land cover map. The AETI product provides an estimate of actual evaporation, transpiration and interception.

2.1.5 SSEBop

SSEBop Version 6 (SSEBop) (Senay et al., 2022) applies the principle of satellite psychrometry using the FANO algorithm (Senay et al., 2023) to integrate VIIRS thermal imagery, temperature data downscaled from ERA5, ERA5 radiation, and reference ET data calculated from JRA-55 data plus others using Penman-Monteith to provide dekadal ET estimates at a 500 m resolution. The ETa product includes transpiration, soil evaporation and interception losses.

2.2 Reanalysis ET Products

2.2.1 ERA5 Land

ERA5-Land (ERA5) (Hersbach et al., 2020) provides hourly ET estimates at a ~9 Km resolution using the ECMWF IFS H-TESSEL land surface model. It utilizes atmospheric forcing from ERA5, MODIS vegetation data, and Global Land Cover Characteristics (GLCC) (Earth Resources Observation And Science (EROS) Center, 2017) derived from AVHRR as inputs.





ERA5-Land provides a "total evaporation" product, which includes evaporation from the earth's surface plus a simple representation of transpiration.

2.2.2 MERRA 2

MERRA-2 (MERRA) (Gelaro et al., 2017) provides hourly estimates at a ~50 x 70 km resolution approximately using NASA's GEOS-5 model with the Catchment Land Surface Model (CLSM), It uses GLCC land cover data, with vegetation inputs from MODIS and Advanced Very High-Resolution Radiometer (AVHRR). The "EVLAND" variable from the M2T1NXLND collection includes transpiration, evaporation from bare soil and intercepted water.

2.2.3 GLDAS

GLDAS (GLDAS) (Rodell et al., 2004) daily CLSM provides ET estimates at a ~27 km resolution using the CLSM model version 2.2 within the Land Information System (LIS) Version 7. It is forced with ECMWF IFS meteorological fields and incorporates UMD land cover classification scheme (Hansen et al., 2000) from AVHRR with MODIS vegetation data and GRACE data assimilation, the variable "Evap_tavg" from the GLDAS CLSM025_D dataset is used. This variable encompasses both evaporation from the land surface and transpiration from plants.

2.2.4 JRA_3Q

JRA-3Q (JRA) (Japan Meteorological Agency, 2023) is based on the TL479 version of JMA's NWP system. It provides hourly ET estimates at a ~40 km resolution using the Simple Biosphere model (SiB) land surface scheme. It incorporates forcing fields from previous JMA JRA-55 reanalysis dataset and satellite data from various sensors including MODIS, AVHRR, and Meteosat. latent heat net flux (lhtfl1have-sfc-fc-gauss) from the 0.375 degrees grid dataset was used which represents total ET from land surface.

135 2.3 Validation (Field) data

140

Actual ET estimates are not yet readily available in Ireland despite the expansion of a flux tower network (Richards et al., 2023). Historically, a network of weighing lysimeters was used to estimate actual ET from grass but this network was discontinued/ceased in 2015 (Donegan, 2024). In the absence of actual ET estimates, meteorological data are often used in combination with the Penman-Monteith formulation for reference ET (ET_o) and crop coefficients to provide such estimates.

The Penman-Monteith equation (Allen et al., 1998) provides an estimate of ET for a specific reference crop (ET_o) e.g. grass, experiencing no stress. ET_o is converted to a crop specific actual ET using a single (K_c) or dual (K_cK_s) crop coefficient. The K_c value is a function of the crop type and the stage of growth and K_s introduce crop stress conditions.





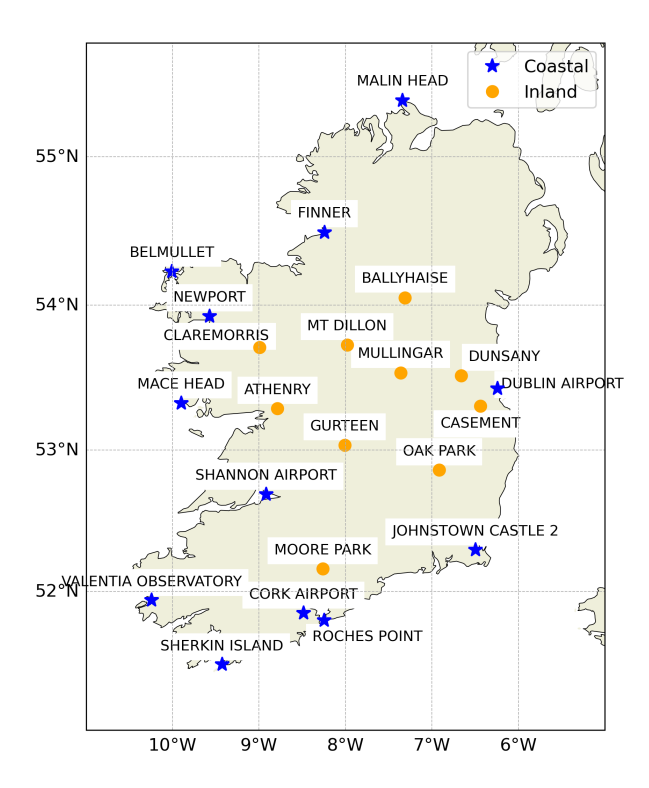


Figure 1. Spatial distribution and geographical location of field data points that were used for ET calculations and data extraction of ET products.

- In this study, meteorological data from 22 selected stations located across Ireland (Figure 1), installed according to standard conditions (well-watered short grass surface), were used to estimate reference grass ET_o according to Allen et al. (1998). Figure 2 shows an image of the weather station at Valentia Observatory installed above managed short grass, one of the 22 weather observing stations used in this study.
- For methodology development under well-maintained synoptic station conditions, $K_s = K_c = 1$ (denoting no water stress and alignment with the reference grass standard) are justified, as the crop environment matches the idealized ET_o conditions. We therefore assume the grass reference ET_o represents actual ET from the grass surface at these stations (ET = ET_o).







Figure 2. Valentia Observatory, one of Met Éireann's 22 synoptic weather stations.

3 Methods

160

165

5 3.1 Data Preparation

3.1.1 Validation Data

The variables required to calculate the ET validation dataset using the PM equation were obtained from daily and hourly files downloaded from Met Éireann's historical data (MetÉireann, 2025). Daily data included maximum temperature, minimum temperature, wind speed, and global radiation, while relative humidity was provided at an hourly resolution. However, some data gaps were present during the five-year study period.

Missing data were identified for all variables: maximum and minimum temperature (4 days), wind speed (11 days), and relative humidity (4 days). Additionally, global radiation was not measured at three stations (Casement, Cork Airport, and Shannon Airport), and where measurements were available, 72 days of data were missing.

To address these gaps, different gap-filling approaches were applied. For missing maximum temperature, minimum temperature, wind speed, and relative humidity values, daily climatological averages were used. In the case of global radiation, two methods were employed: at the three non-measuring stations, radiation was estimated from sunshine hours following Allen et al. (1998) recommendations; for the 72 missing days where sunshine data were also unavailable, radiation was calculated using air temperature differences following the method described in Allen et al. (1998).

The equation with specific parameters to estimate Penman-Monteith ET for short well-watered grass (Allen et al., 1998) was used in this study using the gapfilled datasets of daily and hourly meteorological data for all stations and for the entire period.





Table 1. Spatial and temporal resolution of products

Product	Spatial Resolution (km)	Temporal Resolution
MERRA	\sim 69.375 × \sim 55.5	Hourly
JRA	\sim 41.625 \times \sim 138.75	Hourly
GLDAS	\sim 27.75 \times \sim 27.75	Daily
ERA5	9×9	Daily
GLEAM	9×9	Daily
LSA	3×3	Daily
SSEBop	1×1	10-days
AQUA	0.5×0.5	8-days
TERRA	0.5×0.5	8-days
WaPOR	0.3×0.3	10-days

3.1.2 Remote Data

Remote sensing-derived and reanalysis data are available in gridded formats with different spatial resolutions to the field data collected at point locations as shown in Table 1. Additionally, the data were provided in different units. To facilitate data comparison and the development of an optimization methodology (Figure 3), all datasets were standardized to the same geographical locations and units.

The geographical coordinates of each field site (Figure 1) were used to extract corresponding remote sensing and reanalysis data from the nearest pixel in each product. For low-resolution products where the nearest pixel fell over water (shown as 'no data' in the original files), we instead used the closest valid land pixel with available estimates.

All ET estimates were converted to 8-day cumulative values in millimeters (mm), consistent with the MODIS products format widely adopted in ET studies. For hourly and daily estimates, values were summed. 10-day resolution composites were uniformly distributed into daily averages, then reaggregated into 8-day summed totals. Depth estimates in meters (ERA5-Land) were converted to millimeters. Flux estimates (GLDAS and JRA 3Q) were converted to depth equivalents (mm).

All processing, statistical analysis, and model development were performed using Python scripts in a Jupyter Notebook environment, with raw data extracted from remote sensing-based and reanalysis products, as well as calculated ET_o validation data.

Figure 3 illustrates the methodological workflow for generating an optimized ET product by integrating weather station observations with remote sensing and reanalysis data. The process begins with ET calculations using the PM equation based on observations from 22 weather stations. In parallel, ET estimates are extracted from remote sensing (6 products) and reanalysis datasets (4 products) at pixel locations corresponding to the station coordinates. All ET values are then aggregated into 8-day estimates to standardize the temporal resolution. These aggregated values are compared using the PM estimates as the reference or "truth." The comparison results inform an adaptive post-processing method, which consists of an adaptive bias removal step,





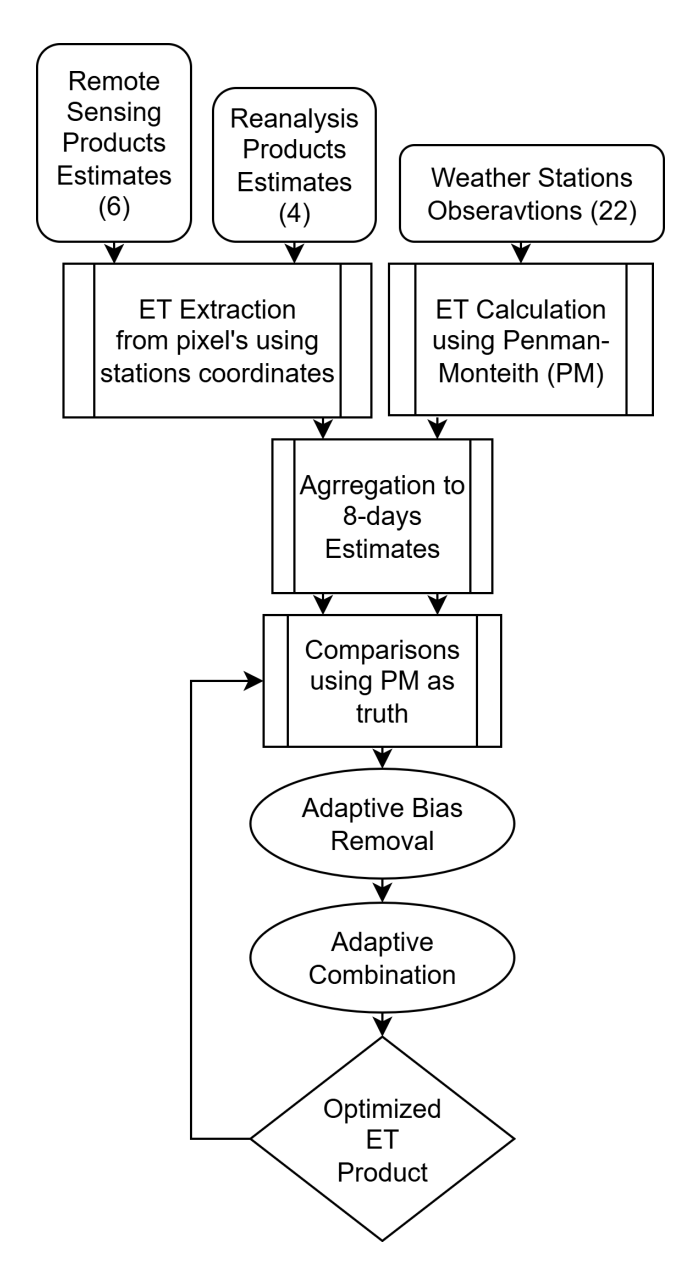


Figure 3. Description of key process followed to prepare data for data comparison and inclusion in the methodology development and analysis.

followed by an adaptive combination of the multiple ET sources. This integration process culminates in the production of an optimized ET product that leverages the strengths of all available data sources while minimizing individual biases.





3.2 Skill Scores

Several statistical measures, including error, bias, root mean square error, and correlation coefficients, were calculated and used as skill scores in the methodology.

200

The error (E) is defined as the difference between the remote estimate (R) and the PM estimate (O). E_j is the error at time j, given by:

$$E_j = R_j - O_j \tag{1}$$

The bias (ME) is the mean of the errors. Where N is the number of observations, the bias is given by:

205
$$ME = \frac{1}{N} \sum_{j=1}^{N} E_j$$
 (2)

The root mean square error (*RMSE*) is the square root of the mean of the squared errors. This is a useful skill sore, as it avoids errors of opposite signs cancelling, and penalises larger errors more heavily. The RMSE is given by:

$$RMSE = \sqrt{\frac{1}{N} \sum_{j=1}^{N} E_j^2} \tag{3}$$

The correlation coefficient (*CC*) is a measure of the linear relationship between the remote and PM estimates. The CC is given by:

$$CC = \frac{\sum_{j=1}^{N} (R_j - \bar{R})(O_j - \bar{O})}{N\sigma_B \sigma_O} \tag{4}$$

where \bar{R} and \bar{O} are the mean values, and σ_R and σ_O are the standard deviations of the remote and PM estimates, respectively.

3.3 Adaptive Post-processing

The adaptive post-processing approach is considered in two parts.

215 3.3.1 Adaptive Bias Removal

220

The first part aims to remove the seasonal bias from the ET estimates using an adaptive bias removal (AB) method. This correction is applied by using a rolling mean of errors over different time windows (iw) each representing 8-day periods. The goal was to identify the optimal iw that minimizes the mean error after correction. After testing window sizes ranging from iw = 1 to 8 using the entire dataset, we found that iw = 4 yielded the lowest mean error. Figure 4 demonstrates that this window size effectively reduced systematic biases while maintaining responsiveness to temporal variations, making it the best choice for bias correction. The AB correction is re-calculated at each time step using equation 5, allowing it to adapt to the seasonal cycle and to varying biases across different years.





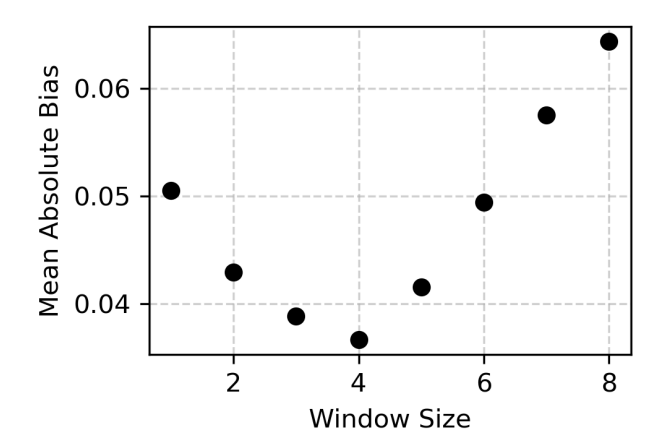


Figure 4. Mean error plots for each window size using the entire dataset for adaptive bias removal process.

$$AB_j = R_j - \frac{1}{4} \sum_{i=j-4}^{j-1} E_i \tag{5}$$

3.3.2 Adaptive Combination

The second part is the COM method, which combines the individual ET products by generating weights based on their recent errors, following the approach of Sweeney et al. (2013). The error values are squared to avoid cancellation of opposing errors and to penalise larger errors more heavily. A sliding window of the most recent 8 data values (iw = 8) was used to compute the mean of these errors. This window size was selected after testing a range of values, with iw = 8 achieving the best balance between error reduction and responsiveness, as the RMSE decreased and stabilised around this point as shown in Figure 5.

Larger window sizes did not significantly improve RMSE and risked introducing lag in adapting to changing error patterns. The ET products are then combined, using weights which are inversely proportional to their mean errors. There are 10 ET products to combine, and so the weights are calculated using equations (6).

$$err_{i} = (1/8) \sum_{j=1}^{g} err_{(i-j)}^{2}$$

$$w_{i} = \frac{1/err_{i}}{\sum_{i=1}^{10} (1/err_{i})}$$

$$235 \quad COM = \sum_{i=1}^{10} w_{i} AB_{i}$$
(6)

3.4 Relative Performance of ET Products

To capture the spatial and temporal variability in product performance that may be masked by aggregated statistics, we implemented a frequency-based method to assess the relative performance of each ET product. For every station and each day in the





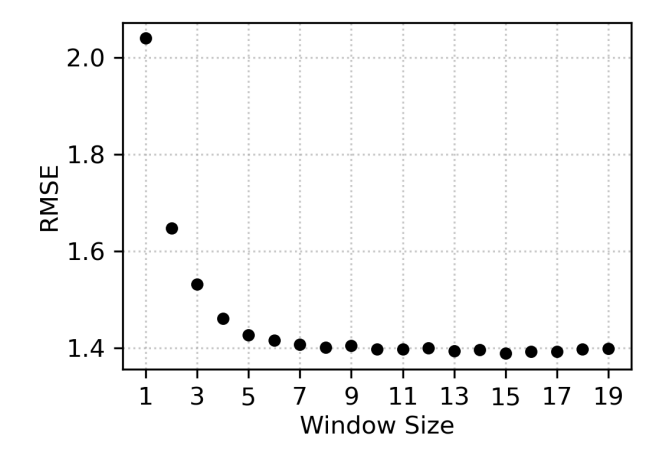


Figure 5. RMSE plots for each window size for adaptive combination process.

study period, the product with the lowest absolute error relative to the PM reference was identified. This daily "best performer" was recorded per station.

For each product, the number of times it ranked as the most accurate was counted at each station and then divided by the total number of time steps for that station. This yielded a station-specific percentage indicating how frequently each product was the most accurate. These percentages were then averaged across all 22 stations to produce an overall value for each product. This method provides a complementary perspective on product performance by highlighting which product performed best most often across different conditions, rather than relying solely on overall statistical metrics.

4 Results

245

250

4.1 Seasonal Variation in ET

Mean ET values for the five years considered (2019–2023), based on data from all 22 sites distributed across Ireland, are shown in Figure 6(a). ET has a strong seasonal cycle, as expected, with higher ET values during the summer, when solar radiation, temperature and vegetation levels are at their highest. Figure 6(b) shows the errors of the remote estimates. The seasonal cycle is clearly visible in the ET values, but also apparent in the errors, with the largest errors in the summer months and the smallest errors in the winter months. The ET estimates are low, characteristic of a cool or temperate maritime climate; relative errors appear to be high.

4.2 Original Skill Scores

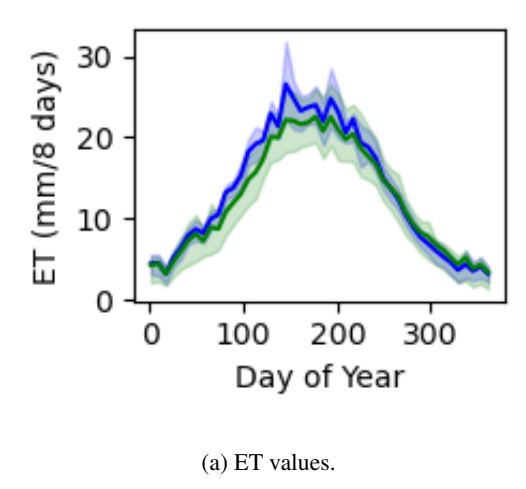
The original skill scores for the ET estimates, averaged across all stations and years, are shown in the Taylor diagram in Figure 7. The diagram concisely compares the 10 remote-based ET products (LSA, GLEAM, ERA5, AQUA, TERRA, GLDAS,



260

265





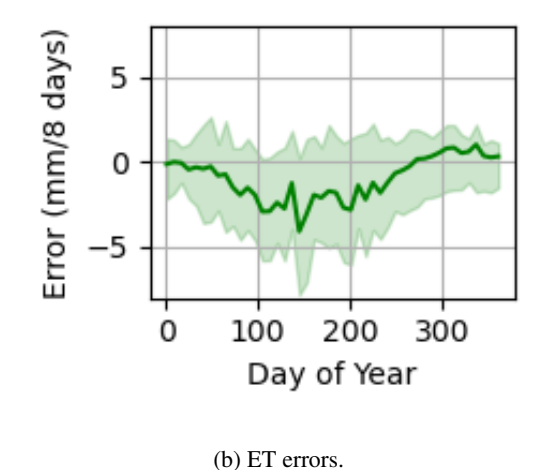


Figure 6. (a) Mean ET estimates from PM (blue) and from Remote sensing Estimates (green) plotted against Day of Year (DOY), for the period 1 January 2019–31 December 2023. (b) ET error estimates plotted against DOY. Shaded areas represent the interquartile ranges. Bold lines represent the mean of the estimates for all stations and all years.

SSEBop, JRA, MERRA, and WaPOR) against the reference dataset (PM) using three key metrics: standard deviation (radial distance from the origin), correlation coefficient (angular position), and centered RMSE (distance from the reference point). These results are based on data from all 22 sites distributed across Ireland over the five-year period from 2019 to 2023.

In the diagram, the dashed arc represents the standard deviation of the reference dataset (PM), providing a visual benchmark for comparing the variability of each product to that of the observations. Products closer to the reference point (PM) along the x-axis exhibit better agreement in magnitude and temporal variability; higher correlations indicate stronger pattern matching, and proximity to the reference point reflects lower errors. This visualization efficiently highlights relative performance, enabling quick identification of the most accurate ET estimates across the entire dataset.

Figure 7 clearly demonstrates that LSA shows the closest agreement with the reference PM model, exhibiting the highest correlation coefficient, lowest centered RMSE, and a standard deviation nearly matching the reference. GLEAM also performs well, with a high correlation coefficient and moderate standard deviation, indicating it reproduces similar temporal patterns but with slightly different magnitudes of ET estimates. Among the other products, AQUA, TERRA, and GLDAS maintain good correlations and relatively low variability, suggesting generally consistent patterns and magnitudes compared to PM. WaPOR, SSEBop, and ERA5 display intermediate performance, with reasonable correlations but more pronounced deviations in standard deviation, reflecting systematic biases in their ET estimates. In contrast, MERRA and JRA show the poorest performance, characterized by weak correlations and either substantial overestimation or underestimation (evident in their higher standard deviations) relative to PM. Overall, LSA and GLEAM stand out as the most reliable ET products, while MERRA and JRA exhibit the largest discrepancies when validated against the PM reference for sites in Ireland.





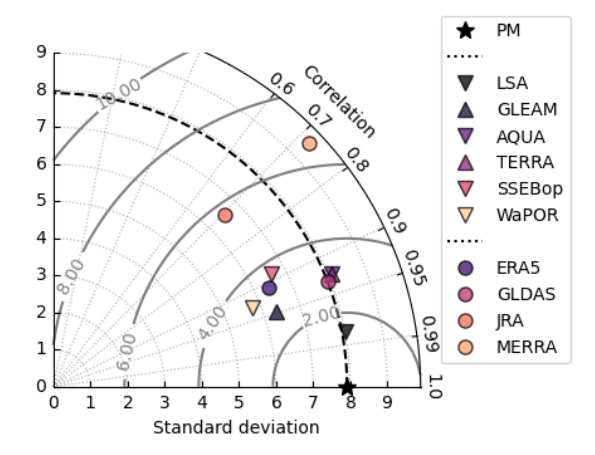


Figure 7. Taylor diagram showing the skill scores for the ET estimates. Circles represent reanalysis products (ERA5, GLDAS, JRA, MERRA), while triangles denote satellite-derived estimates (LSA, GLEAM, AQUA, TERRA, SSEBop, WaPOR).

275 4.3 Adaptive Skill Scores

280

285

The adaptive bias removal method (AB) is applied to each product. Figure 8 shows the mean error for each product at each of the 22 station locations, before and after adaptive bias removal. The green circles show the original mean error at each station, while the black crosses—often overlapping due to values clustering near zero error—represent the mean error after adaptive bias removal. This demonstrates that AB is successful in removing the systematic bias for each product at each station. However, this does not mean that all errors are removed, as underlying positive and negative errors may cancel each other.

The Taylor diagram in Figure 9 shows that the skill scores for all products have improved, compared with their original scores (Figure 7). Products have moved close to the dashed line, which represents the standard deviation of the PM values, showing that correlation has improved for all products. Some products have also shown a reduction in their centred RMSE values, seen by the product markers moving closer to the PM star on the x-axis.

4.4 Relative Performance of ET Products

Figures 7 and 9 both show that the LSA product has the best overall performance before and after AB. However, this aggregate view can obscure the day-to-day and location-specific variability in accuracy.

To explore this variability, we applied the frequency-based method to track how often each product was the most accurate on a given day at each station. The summary results are presented in Figure 10, where values reflect the average percentage of time a product ranked as the best performer across all stations. For instance, LSA's 19.5% indicates it was the most accurate product in about 19.5% of all station-day combinations.





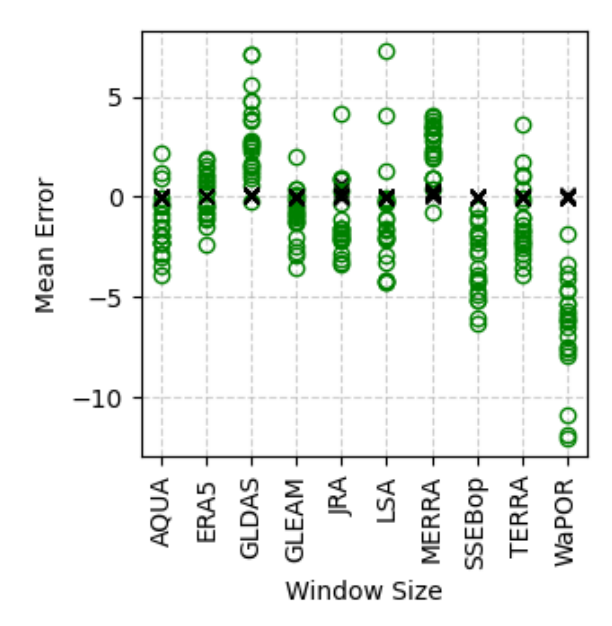


Figure 8. Mean Error for each product at each station. Green circles are for the original data. Black crosses are after adaptive bias removal.

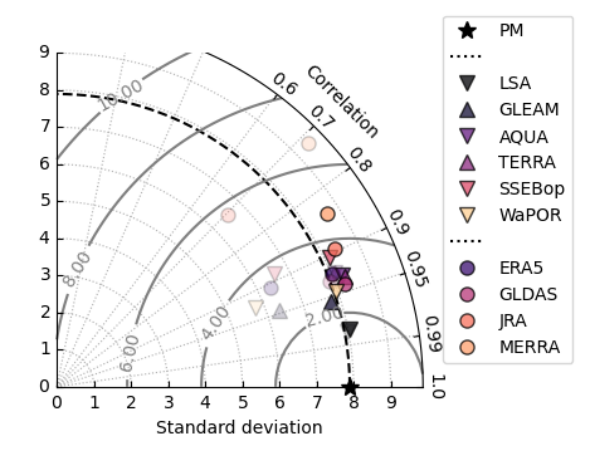


Figure 9. Taylor diagram showing skill scores for original products (transparent) and products after AB (solid).

The results show that no product consistently outperformed all others. Rather, the top-performing product varied across time and space. Before AB, some products like GLEAM and LSA dominated at particular stations. After AB correction, these localized advantages were reduced, and LSA emerged as a consistently strong performer across geographically diverse locations.





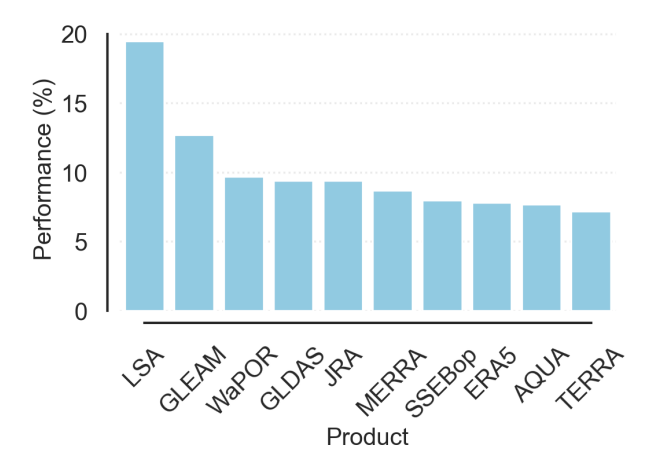


Figure 10. Relative performance of ET products after adaptive bias correction, expressed as percentage of times each product achieved lowest error across the 22 stations for the study period.

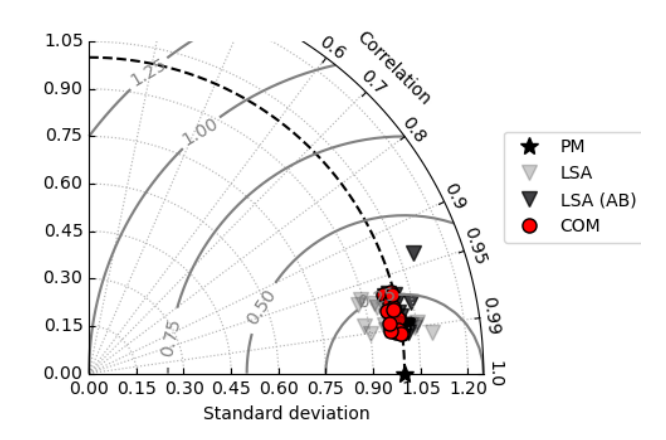


Figure 11. Taylor diagram showing skill scores at each station location for original LSA (transparent blue triangles), *AB* LSA (solid blue triangles) and *COM* (red circles) ET products.

4.5 Combined Product Scores

300

To leverage this complementary behavior, the COM method was developed, generating a new ET product that synthesizes all inputs from all products, weighted by their recent skill performance. This approach systematically combines the strengths of each individual product to achieve superior estimation accuracy that no single product achieves alone.

Figure 11 shows the Taylor diagram for the best-performing single product (LSA) and the *COM* product at each station location. Transparent triangles show the scores for the original LSA data, filled triangles show the scores for LSA after *AB*-correction, and circles show the scores for the *COM* product. The *COM* product is an improvement on the *AB* LSA product.



310

315

320



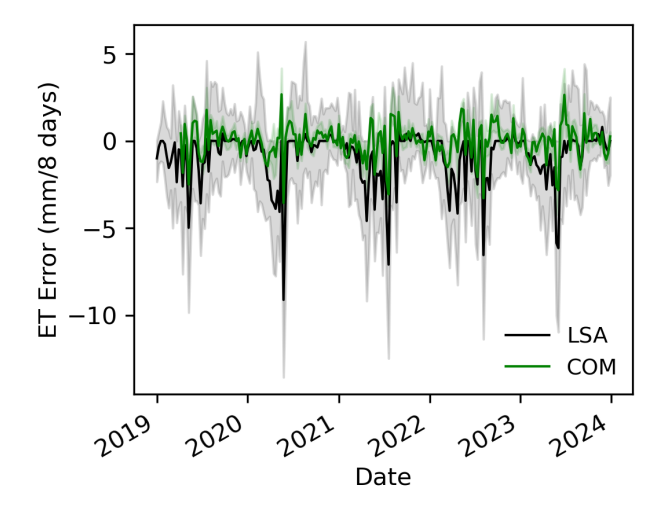


Figure 12. Time series plot comparing ET errors from LSA (black) and *COM* (green) ET products. Bold lines represent the mean of the errors, and shaded areas represent the interquartile ranges.

The overall RMSE skill scores, averaged across all stations, are reduced from 2.94 for the original LSA product to 1.47 for the 305 *AB* LSA product, and to 1.40 for the *COM* product.

Figure 12 compares the seasonal ET error patterns of the LSA and COM products relative to PM estimates from all stations. The error values reveal key differences in performance. The COM product generally maintains lower and more stable errors throughout the period, particularly during peak ET seasons, suggesting better consistency with PM estimates. In contrast, the LSA product exhibits greater error variability, with more pronounced spikes that correspond to periods of high vegetation activity or rapid environmental changes. This comparison highlights COM's superior error mitigation, likely attributable to its multi-source data fusion approach compared to LSA's single-algorithm methodology.

Figure 13 presents a seasonal comparison of ET product performance, distinguishing between Original ET products, AB products, and the COM product. The upper panel shows the average percentage of time the top-performing product from the Original and AB categories was the best per season, along with the average percentage of time the COM product was the best when compared to all products from both categories.

The COM product consistently outperforms the best-performing Original and AB products across all seasons, with particularly strong performance in summer and autumn, where it is the top product nearly 30% of the time. The bottom panel shows the MAE for each category. The COM product again performs best, achieving the lowest MAE in every season, followed by the AB products and then the Original products. These results demonstrate the effectiveness of the AB correction and highlight the COM product's superiority in both consistency and accuracy under varying seasonal conditions.





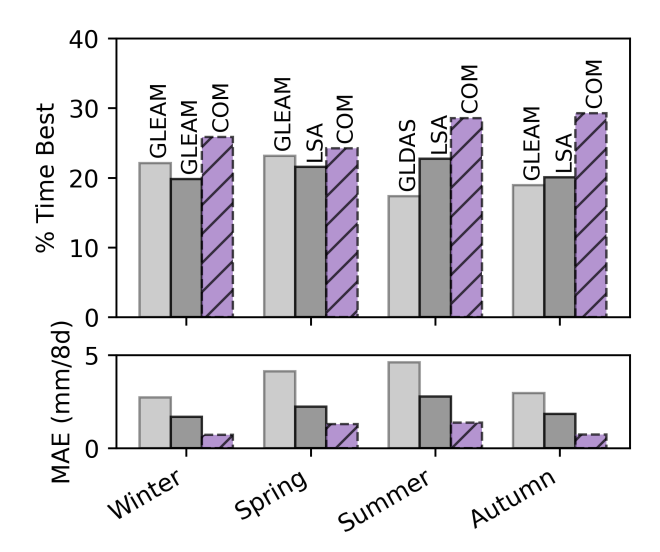


Figure 13. Comparison of seasonal performance metrics for Original, AB, and COM products. The upper panel shows the average percentage of time each product ranks as the best (higher is better) across four seasons (Winter, Spring, Summer, Autumn). Labels above bars indicate the top-performing product for each season. The lower panel presents the MAE in millimeters over 8-day periods for the same products and seasons (lower is better). Bars are colored consistently across panels: Original (gray, lighter), AB (gray, darker), and COM (purple with hatch). Seasons are arranged horizontally with reduced spacing for compactness.

5 Discussion

325

330

335

5.1 Biases in Remote ET Products

Figure 14 shows the relationship between the spatial and temporal resolution and the RMSE for the different ET products. The analysis reveals no clear relationship between spatial/temporal resolution and RMSE in remote ET products. While finer spatial resolution theoretically improves local accuracy, products like WaPOR, SSEBop, AQUA and TEERA (sub-Km to Km resolution) show higher errors than coarser alternatives like LSA and GLEAM (3 and 9 km respectively). Notably, coarser resolution products inherently represent larger areas that typically contain multiple land use types, while finer resolution products capture more homogeneous land cover conditions. This spatial averaging in coarse resolution products effectively smooths out the variability across different land surface conditions, which could explain why they show smaller RMSE values than finer resolution products that preserve more natural spatial heterogeneity.

Similarly, temporal resolution alone doesn't guarantee accuracy - hourly products (JRA and MERRA) underperform some daily datasets (LSA and GLEAM), though the worst errors occur in the 10 day composites (WaPOR and SSEBop). However, the temporal resolution effect may be less significant than spatial resolution since the 10-day composite values are calculated from daily or sub-daily observations. The primary differences may therefore stem more from spatial representation character-





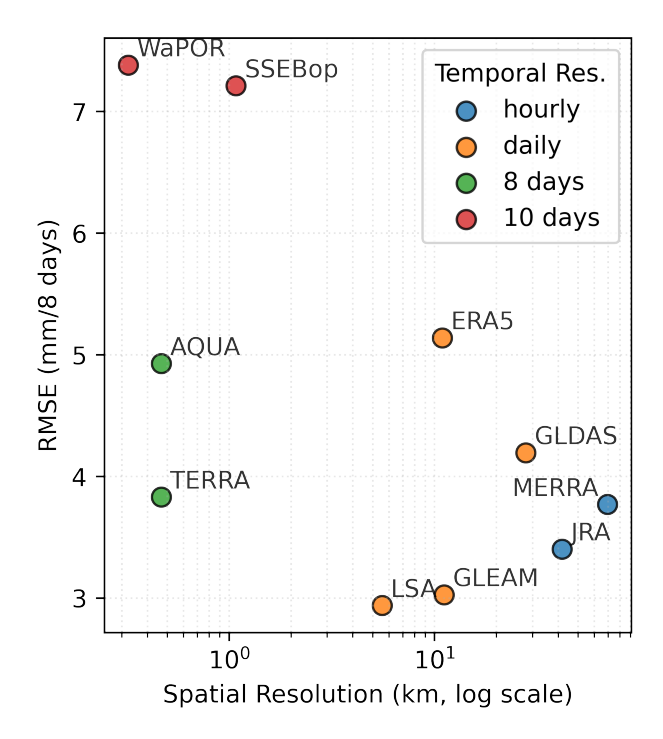


Figure 14. The relationship between the temporal resolution and spatial resolution and the RMSE for the different ET products.

istics than from nominal temporal sampling frequency.

All the ET products examined are based on the same core approach of solving the surface energy balance to estimate latent heat flux and, consequently, ET. Although higher spatial resolution is often assumed to improve accuracy, our analysis showed that this is not necessarily the case. Instead, the main sources of variation in accuracy across products stem from differences in how each model represents vegetation and soil processes, the specific parameterizations used, and the quality of the input data (Cao et al., 2021; Tran et al., 2023). These factors exert a stronger influence on product accuracy than spatial resolution alone. Users should therefore prioritize products that have undergone bias correction and validation, and that are based on high-quality input data, as spatial resolution alone is an unreliable indicator of performance.

345

350

340

Among the ET products analyzed, LSA SAF and GLEAM outperform others overall, primarily due to their incorporation of microwave-based soil moisture observations, which provide a critical advantage over products that rely solely on optical and thermal data. Unlike optical sensors, microwave sensors can penetrate clouds, enabling both LSA SAF and GLEAM to maintain data continuity and accuracy under overcast or rainy conditions. By leveraging soil moisture from sensors such as ASCAT (in both LSA SAF and GLEAM), SMOS, and AMSR2 (in GLEAM), these two products are better equipped to reflect



370



surface water availability and vegetation stress in real time.

In contrast, MODIS Aqua/Terra, WaPOR, and SSEBop rely almost entirely on cloud-sensitive optical and thermal inputs. These include NDVI, LST, albedo, and vegetation indices—parameters that are essential for modeling ET under clear skies but are often unavailable or unreliable under cloud cover. As a result, their ET estimates are more prone to inconsistencies and missing data, particularly in cloudy regions like Ireland. Consequently, the integration of cloud-penetrating microwave soil moisture with frequent optical observations gives LSA SAF—and to a slightly lesser extent GLEAM—a significant advantage in generating consistent and reliable ET estimates across diverse climatic conditions.

Additionally, within this high-performing group, LSA SAF appears to have an edge over GLEAM, likely due to the temporal resolution of their optical data sources. LSA SAF uses inputs from the SEVIRI sensor aboard Meteosat, which delivers 15-minute updates of land surface temperature (LST), albedo, and vegetation indices. This high-frequency data allows LSA SAF to detect short-term fluctuations in surface energy balance and vegetation dynamics, and to adjust ET estimates accordingly. In contrast, GLEAM incorporates optical data from MODIS MOD15A2H, which provides LAI and FAPAR composites at an 8-day temporal resolution. While GLEAM's strength lies in its detailed water balance modeling and robust use of microwave inputs, the infrequent updates from MODIS may reduce its sensitivity to rapidly changing conditions.

Similarly, the reanalysis-based ET products—ERA5-Land, GLDAS, JRA-3Q, and MERRA-2—also exhibited lower performance in comparison to LSA SAF and GLEAM. While these products benefit from data assimilation systems and consistent global coverage, their ET estimates are derived primarily from land surface models driven by atmospheric variables such as temperature, humidity, radiation, and wind speed, rather than real-time satellite-based surface observations. This often leads to smoothed or generalized representations of surface conditions. Moreover, reanalysis systems may incorporate satellite-derived vegetation indices or radiation inputs that are based on optical imagery acquired only under clear-sky conditions, which introduces a bias toward fair-weather estimates and reduces sensitivity to cloudy or variable atmospheric conditions. As a result, their ET outputs tend to be less responsive to short-term fluctuations in land surface conditions, leading to biases particularly in cloudy or heterogeneous regions like Ireland, similar to the limitations seen in optical-only products like MODIS Aqua/Terra, WaPOR, and SSEBop.

As shown in Figure 15(a), remote products exhibit systematically higher errors (RMSE mean: 5.23 and RMSE median: 4.61) in coastal stations compared to inland stations (RMSE mean: 3.80 and RMSE median: 3.16). This performance gap persists across nearly all products, regardless of their spatial resolution. These statistics were calculated across all data from the 22 stations (12 coastal and 10 inland) over the five-year period from 2019 to 2023. Two primary factors contribute to this discrepancy:

1. Mixed pixel effects: A key driver of model error is the presence of mixed land cover types within individual pixels, which complicates signal interpretation and degrades accuracy. In coastal stations, this often involves water bodies that introduce





spectral contamination and boundary effects. Visual analyses showed that high-error coastal stations frequently contained a substantial proportion of water pixels. However, mixed signals are not limited to coastal areas or to water alone. Urban land cover also contributes to retrieval errors due to its complex thermal and surface properties. For example, Casement—an inland station with the highest RMSE among non-coastal sites—was found to have a high percentage of urban pixels across several products. This suggests that urban-induced mixed pixel effects can significantly affect model performance regardless of proximity to the coast. These heterogeneous land cover conditions challenge both high- and low-resolution products, as they obscure the surface characteristics needed for accurate ET estimation.

2. Challenging coastal environments: Even in the absence of mixed land cover, coastal stations pose inherent challenges for evapotranspiration modeling. Conditions such as strong and variable winds, rapid humidity shifts, and maritime influences create dynamic microclimates that standard remote sensing algorithms and physically based models struggle to capture. These atmospheric complexities introduce further uncertainty independent of land type.

The persistent coastal-inland gap across nearly all products underscores that current algorithms systematically underperform in environments where land cover heterogeneity—such as water or urban infrastructure—interacts with natural surfaces (Faridatul et al., 2020). This represents a critical limitation for accurate ET estimation in both coastal and urban-influenced inland settings. Notably, the COM product successfully mitigated this gap, as demonstrated in Figure 15(b) . The mean RMSE difference between coastal and inland stations (Δ (Coastal-Inland)) was reduced from 1.4 mm/8days with original data to just 0.4 mm/8days from the COM product.

5.2 RS and reanalysis data for cloudy environments

Several remote sensing—based ET algorithms rely on multiple inputs like visible to near-infrared (VNIR) satellite derived products, including surface albedo, LST, emissivity, land cover; key biophysical parameters (leaf area index and fractional vegetation cover) (Zhang et al., 2016; Li et al., 2021) and methods of scaling instantaneous to daily estimates (Li et al., 2009).

Cloud cover often limits optical sensors by obscuring land surface properties, resulting in missing LST data and gaps in ET estimates that require infilling with several approaches to do this (Tran et al., 2023).

Some studies have integrated microwave observations — e.g soil moisture and LST—into satellite ET models which also show promise in reducing cloud-induced uncertainties and improving ET accuracy under all-sky conditions (Wang et al., 2022b).

Satellite passive microwave measurements can penetrate cloud cover and are sensitive to variations in vegetation water content over vegetated surfaces (Wang et al., 2022b).

In addition to surface variables, core meteorological drivers of ET — including net radiation, air temperature, and relative humidity — are modulated by cloud cover. This affects both their magnitude and spatial distribution, leading to increased uncertainty in satellite and model-derived ET estimates under variable cloud conditions. Several studies have investigated this (Wang et al., 2022b).

Our study area (Ireland) is characterized by frequent and persistent cloud cover. Ireland experiences complete cloud cover for more than 50% of the time and has an average, hourly cloud cover range of between five and six oktas (Met Éireann, 2025).

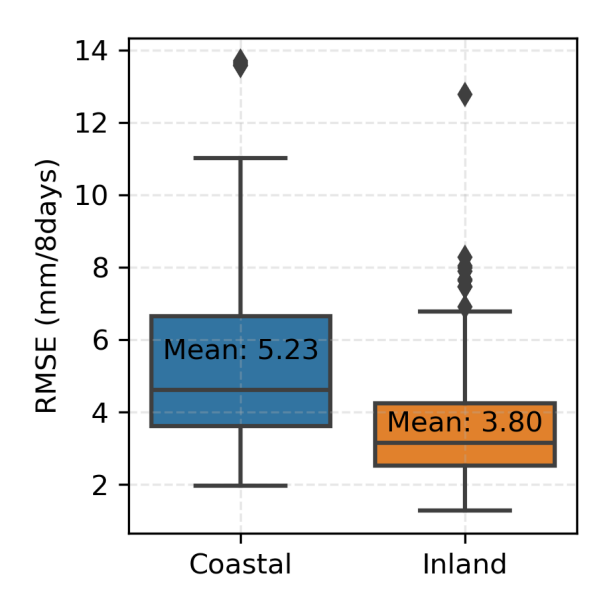


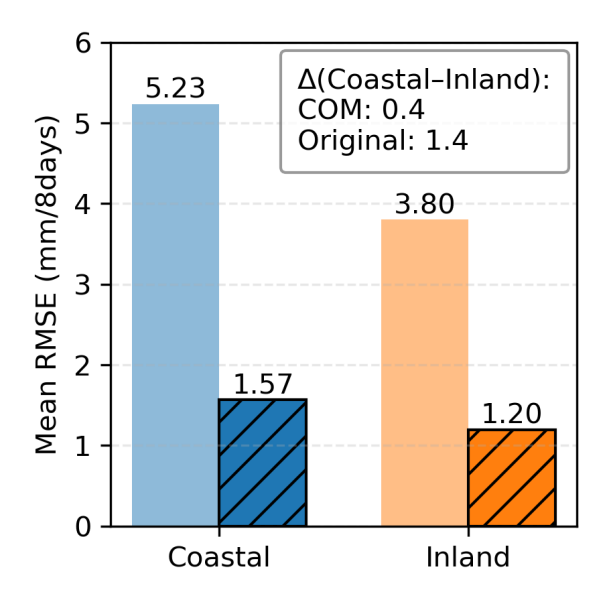
425

430

435







- (a) Remote products RMSE comparison: coastal vs. inland stations.
- (b) RMSE comparison between original remote products and COM product: coastal vs. inland stations.

Figure 15. (a) Box plots of RMSE for coastal stations (blue) versus inland stations (orange). (b) RMSE comparison between: original coastal (transparent blue) and inland (transparent orange) stations, and COM coastal (hatched blue) and COM inland (hatched orange) stations.

420 It is important to take note of the impact of cloud cover on the accuracy of satellite derived ET estimates and derived input climatic variables. Our study used ET product datasets as provided, without examining data infilling methods, or assessing the impact of cloud cover on data accuracy. To our knowledge no assessment has been done for Ireland.

Although the impact of cloud cover on the availability of ET data derived from VNIR data is generally widely acknowledged, few studies have documented this. The recent study by Wang et al. (2023) aims to do this for global ET data products. They also assessed the impact of cloud cover on key drivers of ET, like radiation, temperature, and humidity highlighting the importance of accounting for all-sky conditions in ET modelling and evaluation.

Wang et al. (2023) evaluated seven ET data sets from satellite microwave and optical models, atmospheric reanalysis and land surface models (EDVI, GLEAM, GLASS, MOD16, ERA5, NOAH, CLSM) against eddy covariance flux tower observation from 20 stations located over East Asia. They showed that under heavy cloud conditions, the data products evaluated overestimated ET and produced large bias errors in ET changes (73.82% for EDVI to 159.75% for CLSM). This was substantially higher than the bias errors in the ET changes for small (-40.16 to 8.6%) and moderate cloud changes (-5.39 to 42.91%). Of the data products evaluated by Wang et al. (2023), the satellite microwave-based ET (EDVI) maintained overall lower bias errors and a stable accuracy under all-sky conditions (clear sky to heavily cloudy sky). They highlighted the impact of bias errors in ET under heavy cloud conditions for dense vegetation. The study by Wang et al. (2023) further evaluated the impact of the accuracy of climatic variables, specifically radiation, temperature and humidity, on ET accuracy for all-sky conditions



445

450



and how it impacts different land uses. They highlight that overestimations in incoming shortwave radiation under cloudy conditions, negatively impact ET accuracy.

In addition, Wang et al. (2023) noted that errors in ET may not only be due to the impact of data inputs and clouds, but also by model physical representations.

440 5.3 Static and ML vs Adaptive Methodologies

The results presented in this study highlight the limitations of traditional static fusion methods and underscore the advantages of our adaptive approach in producing more accurate and responsive ET estimates. Static methods such as BMA, STS, TC, and other statistical fusion techniques rely on fixed weighting schemes derived from historical model performance. While these methods are well-established and interpretable, they assume that the relative performance of ET products remains stable over time and space. This assumption does not hold in practice, especially in regions like Ireland, where satellite-based ET estimates are frequently challenged by variable cloud cover, sensor limitations, or seasonal vegetation changes. As a result, static methods can propagate outdated or suboptimal weights, reducing the accuracy of the merged ET product.

In contrast, our adaptive method introduces a dynamic framework that recalibrates product weights based on their most recent performance. This real-time responsiveness ensures that errors from individual datasets are not only identified quickly but also immediately corrected for in the fusion process. The adaptive nature of the method enhances its robustness in the face of shifting observational quality and environmental conditions—factors that are particularly relevant in humid and frequently overcast regions.

The limitations of static methods are echoed in recent work by Zhang and Liang (2020), who fused multiple global forest aboveground biomass (AGB) datasets. Their study demonstrated that conventional weighted averaging methods (e.g., skill-based or independence-weighted averages) failed to account for spatially and temporally varying errors in individual AGB products, resulting in suboptimal fusion (R² = 0.42, RMSE = 88.51 Mg/ha). Instead, they proposed an error removal and dynamic calibration approach, where pixel-level errors in each dataset were estimated using random forest models trained on reference data (e.g., canopy height, climate variables). By dynamically correcting biases before averaging, their fused AGB map achieved significantly higher accuracy (R² = 0.61, RMSE = 53.68 Mg/ha). This aligns with our findings: static weights cannot adapt to localized or transient errors, whereas dynamic recalibration mitigates these issues.

However, while Zhang and Liang (2020)'s use of machine learning (random forests) for error correction improved accuracy, it introduced a layer of complexity: the pixel-level error estimates, though data-driven, are inherently opaque and computationally intensive to generate at scale. This trade-off mirrors broader challenges in adaptive ML frameworks. For instance, Mouatadid et al. (2023) achieved notable success in bias correction for subseasonal forecasts using their Adaptive Bias Correction (ABC) ensemble—a trio of adaptive ML models—yet their method obscures how individual corrections are derived (Mouatadid et al., 2023). In contrast, our method avoids these pitfalls by maintaining full transparency in how weights are





derived and adjusted. It strikes a critical balance between flexibility and explainability, allowing researchers and policymakers to understand and trust the merged product's behavior over time.

These advantages make the proposed adaptive framework a more suitable and forward-looking solution for ET data fusion in dynamic and data-scarce environments.

6 Conclusions

475

480

485

490

495

This study evaluated ten global ET products against PM estimates at 22 Irish stations from 2019 to 2023. All products exhibited systematic and spatially variable errors. The AB correction, which dynamically adjusts each product based on recent errors, reduced the mean RMSE of the best-performing product (LSA-SAF) from 2.94 to 1.47 mm per 8 days. The subsequent COM method, which assigns adaptive weights to each bias-corrected product and merges them into a single combined ET estimate, achieved the lowest overall RMSE (1.40 mm per 8 days). COM consistently outperformed all individual datasets, achieving the lowest MAE in every season and up to 25–30% higher accuracy during summer and autumn—periods of peak ET and greatest product divergence. The framework also narrowed the coastal–inland RMSE gap from 1.4 to 0.4 mm per 8 days, improving consistency under cloudy Irish conditions. Overall, the AB–COM framework provides a transparent, adaptive, and computationally efficient approach to bias correction and data fusion, enhancing ET estimation for operational hydrology, agriculture, and climate monitoring in regions with limited ground data.

7 Future Work

Several international studies (Meng et al., 2024; Salazar-Martínez et al., 2022; Zhu et al., 2022; Guo et al., 2022; Xu et al., 2019) have evaluated the performance of remote sensing-based ET estimates by comparing them with in-situ measurements from eddy covariance flux towers, which are widely regarded as the most direct and reliable method for quantifying actual ET at the ecosystem scale. These studies have provided valuable benchmarks for assessing the accuracy and spatial representativeness of satellite-derived ET products across diverse climatic and land cover conditions. However, such flux tower datasets have not been readily available for Ireland—particularly for the time period considered in this study—posing a key limitation in validating ET estimates in the Irish context. Looking ahead, the emerging data from the National Agricultural Soil Carbon Observatory (NASCO)—a network of eddy covariance towers established since 2020 across representative Irish agricultural landscapes (Richards et al., 2023)—presents a significant opportunity. Once sufficient temporal coverage is achieved, these high-frequency ground-based ET measurements can serve as an independent benchmark to validate and improve ET estimation approaches.



510



The next phase of this research will build on the current work by extending the COM method from site-based analysis to a gridded national-scale application. This will involve generating spatially continuous ET maps across Ireland by applying the COM framework to each pixel, using inputs from remote sensing and reanalysis products. The NASCO flux tower data will be used to correct and validate the spatial performance of the merged product, particularly in agricultural areas. This spatial extension will test the scalability of the COM method and assess its utility in capturing landscape-level ET patterns under Ireland's complex land cover and meteorological conditions. Together, this follow-up work will enhance the operational applicability of the COM framework and contribute to a more robust, high-resolution ET monitoring system for Ireland—supporting national efforts in sustainable water resource management, climate adaptation, and agri-environmental policy development.

Code availability. All global ET products used in this study are publicly available and cited in the manuscript. The derived bias-corrected ET dataset, adaptive bias removal (AB) and merging code (COM), and all scripts for reproducibility are openly accessible on GitHub at: [https://github.com/HaneenMuhammad/ET4I_COM].

Weather station data used for validation were obtained from Met Éireann (Ireland's meteorological service) historical data and are available freely at [https://www.met.ie/climate/available-data/historical-data]. We encourage researchers to use, adapt, and build upon this work, particularly for regions with similar challenges of sparse ground observations and persistent cloud cover. For any questions, please contact the corresponding author.

Author contributions. H.M. was responsible for conceptualization, data curation, formal analysis, methodology, project administration, software, validation, visualization, and writing of the original draft. K.F. contributed to conceptualization, methodology, supervision, and writing of the original draft. P.F. contributed to formal analysis, software development, validation, visualization, and writing of the original draft. G.L. contributed to conceptualization, methodology, and supervision. C.S. contributed to conceptualization, data curation, formal analysis, methodology, software development, supervision, validation, visualization, and writing of the original draft.

Competing interests. The authors declare that they have no conflict of interest.

Acknowledgements. The authors gratefully acknowledge the support provided by Met Éireann (the Irish National Meteorological Service) and Teagasc (the Agriculture and Food Development Authority of Ireland) through the Walsh Scholarship Programme (Scholarship No. 2023201), which co-funded this research. This scholarship supports the *Evapotranspiration for Ireland (ET4I)* project, which aims to produce high-resolution gridded datasets of actual and potential Evapotranspiration across Ireland to support hydrological modeling, agricultural decision-making, and environmental policy.

The authors also acknowledge the use of AI language tools for language editing purposes during manuscript preparation.





References

- Allen, R., Pereira, L., and Smith, M.: Crop Evapotranspiration-Guidelines for Computing Crop Water Requirements-FAO Irrigation and Drainage Paper 56, vol. 56, 1998.
 - Amazirh, A., Er-Raki, S., Chehbouni, A., Rivalland, V., Diarra, A., Khabba, S., Ezzahar, J., and Merlin, O.: Modified Penman–Monteith Equation for Monitoring Evapotranspiration of Wheat Crop: Relationship between the Surface Resistance and Remotely Sensed Stress Index, Biosystems Engineering, 164, 68–84, https://doi.org/10.1016/j.biosystemseng.2017.09.015, 2017.
- Baik, J., Liaqat, U. W., and Choi, M.: Assessment of Satellite- and Reanalysis-Based Evapotranspiration Products with Two Blending Approaches over the Complex Landscapes and Climates of Australia, Agricultural and Forest Meteorology, 263, 388–398, https://doi.org/10.1016/j.agrformet.2018.09.007, 2018.
 - Baik, J., Jeong, J., Park, J., and Choi, M.: Merging Technique for Evapotranspiration Based on In-Situ, Satellite, and Reanalysis Data Using Modifed KGE Fusion Method, Journal of Korea Water Resources Association, 52, 61–70, https://doi.org/10.3741/JKWRA.2019.52.1.61, 2019.
- Cai, J., Liu, Y., Lei, T., and Pereira, L. S.: Estimating Reference Evapotranspiration with the FAO Penman–Monteith Equation Using Daily Weather Forecast Messages, Agricultural and Forest Meteorology, 145, 22–35, https://doi.org/10.1016/j.agrformet.2007.04.012, 2007.
 - Cao, M., Wang, W., Xing, W., Wei, J., Chen, X., Li, J., and Shao, Q.: Multiple Sources of Uncertainties in Satellite Retrieval of Terrestrial Actual Evapotranspiration, Journal of Hydrology, 601, 126 642, https://doi.org/10.1016/j.jhydrol.2021.126642, 2021.
- Champeaux, J.-L., Masson, V., and Chauvin, F.: ECOCLIMAP: A Global Database of Land Surface Parameters at 1 Km Resolution, Meteorological Applications, 12, 29–32, https://doi.org/10.1017/S1350482705001519, 2006.
 - Chen, D., Gao, G., Xu, C., Guo, J., and Ren, G.: Comparison of the Thornthwaite Method and Pan Data with the Standard Penman-Monteith Estimates of Reference Evapotranspiration in China, Climate Research, 28, 123–132, https://doi.org/10.3354/cr028123, 2005.
 - Chen, X., Yao, Y., Li, Y., Zhang, Y., Jia, K., Zhang, X., Shang, K., Yang, J., Bei, X., and Guo, X.: ANN-Based Estimation of Low-Latitude Monthly Ocean Latent Heat Flux by Ensemble Satellite and Reanalysis Products, Sensors, 20, 4773, https://doi.org/10.3390/s20174773, 2020.
 - Cheng, M., Zhong, L., Ma, H., Chang, Y., Li, P., Cheng, M., Wang, X., be, g., and Ma, Y.: A Study on the Assessment and Integration of Multi-Source Evapotranspiration Products over the Tibetan Plateau, Advances in Atmospheric Sciences, 41, 435–448, https://doi.org/10.1007/s00376-023-3036-3, 2024.
- Collatz, G., Ball, J., Grivet, C., and Berry, J. A.: Physiological and Environmental Regulation of Stomatal Conductance, Photosynthesis and Transpiration: A Model That Includes a Laminar Boundary Layer, Agricultural and Forest Meteorology, 54, 107–136, https://doi.org/10.1016/0168-1923(91)90002-8, 1991.
 - Cui, Z., Zhang, Y., Wang, A., Wu, J., and Li, C.: Uncertainty Analysis and Data Fusion of Multi-Source Land Evapotranspiration Products Based on the TCH Method, Remote Sensing, 16, 28, https://doi.org/10.3390/rs16010028, 2023.
 - Donegan, M.: Personal Communication, 2024.
- 560 Earth Resources Observation And Science (EROS) Center: Global Land Cover Characterization (GLCC), https://doi.org/10.5066/F7GB230D, 2017.
 - FAO: WaPOR Database Methodology, FAO, ISBN 978-92-5-132981-8, https://doi.org/10.4060/ca9894en, 2020.
 - Faridatul, M. I., Wu, B., Zhu, X., and Wang, S.: Improving Remote Sensing Based Evapotranspiration Modelling in a Heterogeneous Urban Environment, Journal of Hydrology, 581, 124 405, https://doi.org/10.1016/j.jhydrol.2019.124405, 2020.





- Feng, F., Li, X., Yao, Y., Liang, S., Chen, J., Zhao, X., Jia, K., Pintér, K., and McCaughey, J. H.: An Empirical Orthogonal Function-Based Algorithm for Estimating Terrestrial Latent Heat Flux from Eddy Covariance, Meteorological and Satellite Observations, PLOS ONE, 11, e0160 150, https://doi.org/10.1371/journal.pone.0160150, 2016.
 - García-Gutiérrez, V., Stöckle, C., Gil, P. M., and Meza, F. J.: Evaluation of Penman-Monteith Model Based on Sentinel-2 Data for the Estimation of Actual Evapotranspiration in Vineyards. Remote Sensing, 13, 478, https://doi.org/10.3390/rs13030478, 2021.
- Gelaro, R., McCarty, W., Suárez, M. J., Todling, R., Molod, A., Takacs, L., Randles, C. A., Darmenov, A., Bosilovich, M. G., Reichle, R., Wargan, K., Coy, L., Cullather, R., Draper, C., Akella, S., Buchard, V., Conaty, A., Da Silva, A. M., Gu, W., Kim, G.-K., Koster, R., Lucchesi, R., Merkova, D., Nielsen, J. E., Partyka, G., Pawson, S., Putman, W., Rienecker, M., Schubert, S. D., Sienkiewicz, M., and Zhao, B.: The Modern-Era Retrospective Analysis for Research and Applications, Version 2 (MERRA-2), Journal of Climate, 30, 5419–5454, https://doi.org/10.1175/JCLI-D-16-0758.1, 2017.
- 575 Ghilain, N., Arboleda, A., and Gellens-Meulenberghs, F.: Evapotranspiration Modelling at Large Scale Using Near-Real Time MSG SEVIRI Derived Data, Hydrology and Earth System Sciences, 15, 771–786, https://doi.org/10.5194/hess-15-771-2011, 2011.
 - Ghilain, N., Arboleda, A., Sepulcre-Cantò, G., Batelaan, O., Ardö, J., and Gellens-Meulenberghs, F.: Improving Evapotranspiration in a Land Surface Model Using Biophysical Variables Derived from MSG/SEVIRI Satellite, Hydrology and Earth System Sciences, 16, 2567–2583, https://doi.org/10.5194/hess-16-2567-2012, 2012.
- 580 Guo, X., Meng, D., Chen, X., and Li, X.: Validation and Comparison of Seven Land Surface Evapotranspiration Products in the Haihe River Basin, China, Remote Sensing, 14, 4308, https://doi.org/10.3390/rs14174308, 2022.
 - Guo, X., Yao, Y., Tang, Q., Liang, S., Shao, C., Fisher, J. B., Chen, J., Jia, K., Zhang, X., Shang, K., Yang, J., Yu, R., Xie, Z., Liu, L., Ning, J., and Zhang, L.: Multimodel Ensemble Estimation of Landsat-like Global Terrestrial Latent Heat Flux Using a Generalized Deep CNN-LSTM Integration Algorithm, Agricultural and Forest Meteorology, 349, 109 962, https://doi.org/10.1016/j.agrformet.2024.109962, 2024.
 - Hansen, M. C., Defries, R. S., Townshend, J. R. G., and Sohlberg, R.: Global Land Cover Classification at 1 Km Spatial Resolution Using a Classification Tree Approach, International Journal of Remote Sensing, 21, 1331–1364, https://doi.org/10.1080/014311600210209, 2000.
 He, X., Xu, T., Xia, Y., Bateni, S. M., Guo, Z., Liu, S., Mao, K., Zhang, Y., Feng, H., and Zhao, J.: A Bayesian Three-Cornered Hat (BTCH) Method: Improving the Terrestrial Evapotranspiration Estimation, Remote Sensing, 12, 878, https://doi.org/10.3390/rs12050878, 2020.
- Hersbach, H., Bell, B., Berrisford, P., Hirahara, S., Horányi, A., Muñoz-Sabater, J., Nicolas, J., Peubey, C., Radu, R., Schepers, D., Simmons, A., Soci, C., Abdalla, S., Abellan, X., Balsamo, G., Bechtold, P., Biavati, G., Bidlot, J., Bonavita, M., De Chiara, G., Dahlgren, P., Dee, D., Diamantakis, M., Dragani, R., Flemming, J., Forbes, R., Fuentes, M., Geer, A., Haimberger, L., Healy, S., Hogan, R. J., Hólm, E., Janisková, M., Keeley, S., Laloyaux, P., Lopez, P., Lupu, C., Radnoti, G., De Rosnay, P., Rozum, I., Vamborg, F., Villaume, S., and Thépaut, J.-N.: The ERA5 Global Reanalysis, Quarterly Journal of the Royal Meteorological Society, 146, 1999–2049, https://doi.org/10.1002/qj.3803, 2020.
 - IPCC: Climate Change 2022 Impacts, Adaptation and Vulnerability: Working Group II Contribution to the Sixth Assessment Report of the Intergovernmental Panel on Climate Change, Cambridge University Press, 1 edn., ISBN 978-1-009-32584-4, https://doi.org/10.1017/9781009325844, 2023.
 - Japan Meteorological Agency: Japanese Reanalysis for Three Quarters of a Century (JRA-3Q), https://doi.org/10.5065/AVTZ-1H78, 2023.
- 600 Katul, G. G., Oren, R., Manzoni, S., Higgins, C., and Parlange, M. B.: Evapotranspiration: A Process Driving Mass Transport and Energy Exchange in the Soil-plant-atmosphere-climate System, Reviews of Geophysics, 50, 2011RG000366, https://doi.org/10.1029/2011RG000366, 2012.



605

620



- Kazemi, A., Ghahreman, N., Ghamghami, M., and Ghameshloo, A.: Application of Bayesian Model Averaging (BMA) Approach for Estimating Evapotranspiration in Gorganrood-Gharesoo Basin, Iran, Journal of Agricultural Science and Technology A, 23, 1395–1409, 2021.
- Khattak, W. A., Sun, J., Zaman, F., Jalal, A., Shafiq, M., Manan, S., Hameed, R., Khan, I., Khan, I. U., Khan, K. A., and Du, D.: The Role of Agricultural Land Management in Modulating Water-Carbon Interplay within Dryland Ecological Systems, Agriculture, Ecosystems & Environment, 378, 109 315, https://doi.org/10.1016/j.agee.2024.109315, 2025.
- Li, B., Cui, Y., Geng, X., and Li, H.: Improving the Evapotranspiration Estimation under Cloudy Condition by Extending the Ts-VI Triangle
 Model, Remote Sensing, 13, 1516, https://doi.org/10.3390/rs13081516, 2021.
 - Li, C., Yang, H., Yang, W., Liu, Z., Jia, Y., Li, S., and Yang, D.: Error Characterization of Global Land Evapotranspiration Products: Collocation-based Approach, Journal of Hydrology, 612, 128 102, https://doi.org/10.1016/j.jhydrol.2022.128102, 2022.
 - Li, C., Han, J., Liu, Z., Tu, Z., and Yang, H.: A Harmonized Global Gridded Transpiration Product Based on Collocation Analysis, Scientific Data, 11, 604, https://doi.org/10.1038/s41597-024-03425-7, 2024a.
- 615 Li, C., Liu, Z., Yang, W., Tu, Z., Han, J., Li, S., and Yang, H.: CAMELE: Collocation-Analyzed Multi-source Ensembled Land Evapotranspiration Data, Earth System Science Data, 16, 1811–1846, https://doi.org/10.5194/essd-16-1811-2024, 2024b.
 - Li, X., Zhang, W., Vermeulen, A., Dong, J., and Duan, Z.: Triple Collocation-Based Merging of Multi-Source Gridded Evapotranspiration Data in the Nordic Region, Agricultural and Forest Meteorology, 335, 109 451, https://doi.org/10.1016/j.agrformet.2023.109451, 2023.
 - Li, Z.-L., Tang, R., Wan, Z., Bi, Y., Zhou, C., Tang, B., Yan, G., and Zhang, X.: A Review of Current Methodologies for Regional Evapotranspiration Estimation from Remotely Sensed Data, Sensors, 9, 3801–3853, https://doi.org/10.3390/s90503801, 2009.
 - Lu, J., Wang, G., Chen, T., Li, S., Hagan, D. F. T., Kattel, G., Peng, J., Jiang, T., and Su, B.: A Harmonized Global Land Evaporation Dataset from Model-Based Products Covering 1980–2017, Earth System Science Data, 13, 5879–5898, https://doi.org/10.5194/essd-13-5879-2021, 2021.
- Meng, X., Deng, M., Shu, L., Chen, H., Wang, S., Li, Z., Zhao, L., and Shang, L.: An Evaluation of Evapotranspiration Products over the Tibetan Plateau, Journal of Hydrometeorology, 25, 1665–1677, https://doi.org/10.1175/JHM-D-23-0223.1, 2024.
 - Met Éireann: Sunshine Met Éireann The Irish Meteorological Service, https://www.met.ie/climate/what-we-measure/sunshine, 2025.
 - MetÉireann: Historical Data Met Éireann The Irish Meteorological Service, https://www.met.ie/climate/available-data/historical-data, 2025.
- Miralles, D. G., Bonte, O., Koppa, A., Baez-Villanueva, O. M., Tronquo, E., Zhong, F., Beck, H. E., Hulsman, P., Dorigo, W., Verhoest, N. E. C., and Haghdoost, S.: GLEAM4: Global Land Evaporation and Soil Moisture Dataset at 0.1° Resolution from 1980 to near Present, Scientific Data, 12, 416, https://doi.org/10.1038/s41597-025-04610-y, 2025.
 - Mouatadid, S., Orenstein, P., Flaspohler, G., Cohen, J., Oprescu, M., Fraenkel, E., and Mackey, L.: Adaptive Bias Correction for Improved Subseasonal Forecasting, Nature Communications, 14, 3482, https://doi.org/10.1038/s41467-023-38874-y, 2023.
- Mu, Q., Heinsch, F. A., Zhao, M., and Running, S. W.: Development of a Global Evapotranspiration Algorithm Based on MODIS and Global Meteorology Data, Remote Sensing of Environment, 111, 519–536, https://doi.org/10.1016/j.rse.2007.04.015, 2007.
 - Park, J., Baik, J., and Choi, M.: Triple Collocation-Based Multi-Source Evaporation and Transpiration Merging, Agricultural and Forest Meteorology, 331, 109 353, https://doi.org/10.1016/j.agrformet.2023.109353, 2023.
 - Richards, K. G., Murphy, R., Rambaud, J., Bracken, C., Bishop, J., Gleasure, G., Saunders, M., and Lanigan, G. J.: Establishing the Irish National Agricultural Soil Carbon Observatory (NASCO), in: ASA, CSSA, SSSA International Annual Meeting, ASA-CSSA-SSSA, 2023.



650



- Rodell, M., Houser, P., Jambor, U., Gottschalck, J., Mitchell, K., Meng, J., Arsenault, K., Brian, C., Radakovich, J., MG, B., Entin, J., Walker, J., Lohmann, D., and DL, T.: The Global Land Data Assimilation System, bams, 85, 381–394, https://doi.org/10.1175/BAMS-85-3-381, 2004.
- Salazar-Martínez, D., Holwerda, F., Holmes, T. R., Yépez, E. A., Hain, C. R., Alvarado-Barrientos, S., Ángeles-Pérez, G., ArredondoMoreno, T., Delgado-Balbuena, J., Figueroa-Espinoza, B., Garatuza-Payán, J., González Del Castillo, E., Rodríguez, J. C., Rojas-Robles,
 N. E., Uuh-Sonda, J. M., and Vivoni, E. R.: Evaluation of Remote Sensing-Based Evapotranspiration Products at Low-Latitude Eddy
 Covariance Sites, Journal of Hydrology, 610, 127 786, https://doi.org/10.1016/j.jhydrol.2022.127786, 2022.
 - Senay, G., Friedrichs, M., Morton, C., Parrish, G., Schauer, M., Khand, K., Kagone, S., Boiko, O., and Huntington, J.: Mapping Actual Evapotranspiration Using Landsat for the Conterminous United States: Google Earth Engine Implementation and Assessment of the SSEBop Model, Remote Sensing of Environment, 275, 113 011, https://doi.org/10.1016/j.rse.2022.113011, 2022.
 - Senay, G. B., Parrish, G. E. L., Schauer, M., Friedrichs, M., Khand, K., Boiko, O., Kagone, S., Dittmeier, R., Arab, S., and Ji, L.: Improving the Operational Simplified Surface Energy Balance Evapotranspiration Model Using the Forcing and Normalizing Operation, Remote Sensing, 15, 260, https://doi.org/10.3390/rs15010260, 2023.
- Shang, K., Yao, Y., Li, Y., Yang, J., Jia, K., Zhang, X., Chen, X., Bei, X., and Guo, X.: Fusion of Five Satellite-Derived
 Products Using Extremely Randomized Trees to Estimate Terrestrial Latent Heat Flux over Europe, Remote Sensing, 12, 687, https://doi.org/10.3390/rs12040687, 2020.
 - Simons, G., Koster, R., and Droogers, P.: Hihydrosoil v2. 0-High Resolution Soil Maps of Global Hydraulic Properties, Future Works.[online] Available from https://www. futurewater. eu/projects/hihydrosoil, 2020.
- Song, L., Bateni, S. M., Xu, Y., Xu, T., He, X., Ki, S. J., Liu, S., Ma, M., and Yang, Y.: Reconstruction of Remotely Sensed Daily Evapotranspiration Data in Cloudy-Sky Conditions, Agricultural Water Management, 255, 107 000, https://doi.org/10.1016/j.agwat.2021.107000, 2021.
 - Stap, L. B., Van Den Hurk, B. J. J. M., Van Heerwaarden, C. C., and Neggers, R. A. J.: Modeled Contrast in the Response of the Surface Energy Balance to Heat Waves for Forest and Grassland, Journal of Hydrometeorology, 15, 973–989, https://doi.org/10.1175/JHM-D-13-029.1, 2014.
- 665 Sweeney, C. P., Lynch, P., and Nolan, P.: Reducing Errors of Wind Speed Forecasts by an Optimal Combination of Post-processing Methods, Meteorological Applications, 20, 32–40, https://doi.org/10.1002/met.294, 2013.
 - Tran, B. N., Van Der Kwast, J., Seyoum, S., Uijlenhoet, R., Jewitt, G., and Mul, M.: Uncertainty Assessment of Satellite Remote-Sensing-Based Evapotranspiration Estimates: A Systematic Review of Methods and Gaps, Hydrology and Earth System Sciences, 27, 4505–4528, https://doi.org/10.5194/hess-27-4505-2023, 2023.
- Trigo, I. F., Dacamara, C. C., Viterbo, P., Roujean, J.-L., Olesen, F., Barroso, C., Camacho-de-Coca, F., Carrer, D., Freitas, S. C., García-Haro, J., Geiger, B., Gellens-Meulenberghs, F., Ghilain, N., Meliá, J., Pessanha, L., Siljamo, N., and Arboleda, A.: The Satellite Application Facility for Land Surface Analysis, International Journal of Remote Sensing, 32, 2725–2744, https://doi.org/10.1080/01431161003743199, 2011.
 - Wang, D., Liu, S., and Wang, D.: Triple Collocation-Based Uncertainty Analysis and Data Fusion of Multi-Source Evapotranspiration Data Across China, Atmosphere, 15, 1410, https://doi.org/10.3390/atmos15121410, 2024.
 - Wang, J., Cheng, D., Wu, L., and Yu, X.: Remote-Sensing Inversion Method for Evapotranspiration by Fusing Knowledge and Multisource Data, Scientific Programming, 2022, 1–13, https://doi.org/10.1155/2022/2076633, 2022a.





- Wang, J.-B., Zhao, X.-L., Ye, H., Zhang, Z.-J., and He, H.-L.: Integration of Evapotranspiration Remote Sensing Products Based on Bayesian Model Averaging: An Example from Three-River-Source National Park, The journal of applied ecology, 32(6), 2021a.
- Wang, L., Wu, B., Elnashar, A., Zeng, H., Zhu, W., and Yan, N.: Synthesizing a Regional Territorial Evapotranspiration Dataset for Northern China, Remote Sensing, 13, 1076, https://doi.org/10.3390/rs13061076, 2021b.
 - Wang, Y., Li, R., Hu, J., Fu, Y., Duan, J., Cheng, Y., and Song, B.: Evaluation of Evapotranspiration Estimation under Cloud Impacts over China Using Ground Observations and Multiple Satellite Optical and Microwave Measurements, Agricultural and Forest Meteorology, 314, 108 806, https://doi.org/10.1016/j.agrformet.2021.108806, 2022b.
- Wang, Y., Hu, J., Li, R., Song, B., Hailemariam, M., Fu, Y., and Duan, J.: Increasing Cloud Coverage Deteriorates Evapotranspiration Estimating Accuracy From Satellite, Reanalysis and Land Surface Models Over East Asia, Geophysical Research Letters, 50, e2022GL102706, https://doi.org/10.1029/2022GL102706, 2023.
 - Wanniarachchi, S. and Sarukkalige, R.: A Review on Evapotranspiration Estimation in Agricultural Water Management: Past, Present, and Future, Hydrology, 9, 123, https://doi.org/10.3390/hydrology9070123, 2022.
- Westerhoff, R.: Using Uncertainty of Penman and Penman–Monteith Methods in Combined Satellite and Ground-Based Evapotranspiration Estimates, Remote Sensing of Environment, 169, 102–112, https://doi.org/10.1016/j.rse.2015.07.021, 2015.
 - Xu, T., Guo, Z., Xia, Y., Ferreira, V. G., Liu, S., Wang, K., Yao, Y., Zhang, X., and Zhao, C.: Evaluation of Twelve Evapotranspiration Products from Machine Learning, Remote Sensing and Land Surface Models over Conterminous United States, Journal of Hydrology, 578, 124105, https://doi.org/10.1016/j.jhydrol.2019.124105, 2019.
- Yao, Y., Liang, S., Li, X., Hong, Y., Fisher, J. B., Zhang, N., Chen, J., Cheng, J., Zhao, S., Zhang, X., Jiang, B., Sun, L., Jia, K., Wang, K., Chen, Y., Mu, Q., and Feng, F.: Bayesian Multimodel Estimation of Global Terrestrial Latent Heat Flux from Eddy Covariance, Meteorological, and Satellite Observations, Journal of Geophysical Research: Atmospheres, 119, 4521–4545, https://doi.org/10.1002/2013JD020864, 2014.
- Yao, Y., Liang, S., Li, X., Liu, S., Chen, J., Zhang, X., Jia, K., Jiang, B., Xie, X., Munier, S., Liu, M., Yu, J., Lindroth, A., Varlagin, A., Raschi,
 A., Noormets, A., Pio, C., Wohlfahrt, G., Sun, G., Domec, J.-C., Montagnani, L., Lund, M., Eddy, M., Blanken, P. D., Grünwald, T., Wolf,
 S., and Magliulo, V.: Assessment and Simulation of Global Terrestrial Latent Heat Flux by Synthesis of CMIP5 Climate Models and Surface Eddy Covariance Observations, Agricultural and Forest Meteorology, 223, 151–167, https://doi.org/10.1016/j.agrformet.2016.03.016, 2016.
- Yao, Y., Liang, S., Li, X., Zhang, Y., Chen, J., Jia, K., Zhang, X., Fisher, J. B., Wang, X., Zhang, L., Xu, J., Shao, C., Posse, G., Li, Y.,
 Magliulo, V., Varlagin, A., Moors, E. J., Boike, J., Macfarlane, C., Kato, T., Buchmann, N., Billesbach, D., Beringer, J., Wolf, S., Papuga,
 S. A., Wohlfahrt, G., Montagnani, L., Ardö, J., Paul-Limoges, E., Emmel, C., Hörtnagl, L., Sachs, T., Gruening, C., Gioli, B., LópezBallesteros, A., Steinbrecher, R., and Gielen, B.: Estimation of High-Resolution Terrestrial Evapotranspiration from Landsat Data Using
 a Simple Taylor Skill Fusion Method, Journal of Hydrology, 553, 508–526, https://doi.org/10.1016/j.jhydrol.2017.08.013, 2017.
- Zhang, K., Kimball, J. S., and Running, S. W.: A Review of Remote Sensing Based Actual Evapotranspiration Estimation, WIREs Water, 3, 834–853, https://doi.org/10.1002/wat2.1168, 2016.
 - Zhang, Y. and Liang, S.: Fusion of Multiple Gridded Biomass Datasets for Generating a Global Forest Aboveground Biomass Map, Remote Sensing, 12, 2559, https://doi.org/10.3390/rs12162559, 2020.
 - Zhu, G., Li, X., Zhang, K., Ding, Z., Han, T., Ma, J., Huang, C., He, J., and Ma, T.: Multi-Model Ensemble Prediction of Terrestrial Evapotranspiration across North China Using Bayesian Model Averaging: Multi-Model Prediction of Terrestrial ET Using BMA, Hydrological Processes, 30, 2861–2879, https://doi.org/10.1002/hyp.10832, 2016.





Zhu, W., Tian, S., Wei, J., Jia, S., and Song, Z.: Multi-Scale Evaluation of Global Evapotranspiration Products Derived from Remote Sensing Images: Accuracy and Uncertainty, Journal of Hydrology, 611, 127 982, https://doi.org/10.1016/j.jhydrol.2022.127982, 2022.